

A Mixture-of-Gradient-Experts Framework for Accelerating AC Optimal Power Flow

Shourya Bose , Kejun Chen , and Yu Zhang , *Member, IEEE*

Abstract—This paper introduces a novel data-driven constraint screening approach aimed at accelerating the solution of convexified AC optimal power flow (C-OPF) by eliminating non-binding constraints. Our constraint screening process leverages a novel mixture-of-experts architecture called MoGE (Mixture of Gradient Experts), which is trained to predict optimal dual variables based on problem parameters. The results demonstrate that subject to certain mild conditions on the C-OPF model, our proposed method guarantees an identical solution to the full problem but significantly reduces computational time. The solution’s accuracy is shown through C-OPF properties. Even with incorrectly screened constraints, a recovery process is possible. This results in a problem with fewer constraints than the original. Extensive simulations conducted on the quadratic-convex model show that our method outperforms other constraint screening techniques.

I. INTRODUCTION

The Optimal Power Flow (OPF) determines the optimal settings for control variables in an electric power network. Its primary goal is to minimize the total generation cost while satisfying various operational constraints (e.g., generation limits, voltage limits, and line capacity limits). Increasing stochastic factors such as load demand fluctuations and varying generation from renewable distributed energy resources (DERs) necessitate rapid and accurate solutions to large-scale OPF problems. Convexified formulations of AC optimal power flow (ACOPF), which we denote by C-OPFs, have recently gained significant research and industrial attention. C-OPF formulations benefit from theoretical guarantees of global optimality [1] and the availability of mature commercial solvers. Popular C-OPF formulations include DC optimal power flow (DCOPF) [2], DistFlow OPF [3], [4], [5], semidefinite relaxation (SDR) [6], [7], [8], second-order cone programming (SOCP) relaxation [9], quadratic-convex relaxation [10], McCormick relaxation [11], etc. A comprehensive review of those convex approximations can be found in [12].

In this paper, we aim to reduce the solution time of C-OPF solvers using methods that are agnostic to the underlying optimization algorithm. This is achieved by using *Constraint Screening* (CS), which identifies and eliminates constraints that are non-binding at the optimum, thereby reducing problem size and accelerating solution times. Our CS approach uses machine learning to eliminate constraints based on varying load demands and possibly other problem parameters.

This work was partially supported by the 2023 CITRIS Interdisciplinary Innovation Program (I2P).

All authors are with the Department of Electrical and Computer Engineering at the University of California, Santa Cruz, USA. Emails: {shbose, kchen158, zhangy}@ucsc.edu

A. Prior Work

Earliest works on the removal of redundant and non-binding constraints are for linear programs [13], [14]. Recent domain-specific CS methods for power systems are based on geometry of the feasible set or machine learning techniques. CS methods based on feasible set geometry analyze the constraints *a priori* to generate a list of constraints which are provably non-binding at the optimum. Various algorithms are proposed to eliminate redundant line flow constraints for DCOPF formulations, based on solving auxiliary optimization problems [15], [16], [17]. Different methods are developed to accelerate the branch-and-bound algorithm for unit commitment by eliminating network constraints [18], [19], [20], [21].

Machine learning based CS methods leverage historical or synthetic OPF datasets to train learning models, with load demands typically included as key input variables. For example, Deka and Misra [22] and Hasan and Kargarian [23] train deep neural network (DNN) based classifiers to learn the mapping between problem parameters and the binding constraints directly. Dual variables play a pivotal role in DNN applications for OPF, as their optimal values reveal the binding status of corresponding constraints [24], [25]. Chen *et al.* [26] learn optimal dual variables with DNNs to solve DCOPF via solving the dual problem. Nellikath & Chatzivasileiadis [27] leverage the Kahrush-Kuhn-Tucker (KKT) system to improve the robustness of deep learning for learning optimal solutions.

B. Contribution

Based on learning the dual variables, we propose a CS method to reduce the size of C-OPF problems in this paper. We first represent C-OPF as a parametric convex optimization problem with parameters representing values such as load demands and line flow limits, etc. We develop a novel neural network architecture called *MoGE* (*Mixture of Gradient Experts*) to learn the mapping from parameters to optimal dual variables. Once trained, MoGE predicts optimal dual variables for new C-OPF instances, enabling the identification of non-binding constraints via complementary slackness. Removing these non-binding constraints reduces the problem size, thereby accelerating the solution process. In addition, we address the issue of potentially misclassified constraints by incorporating a recovery process. Any identified violated constraints after solving the reduced C-OPF are retroactively added to the active constraints, and the problem is resolved. We demonstrate that the convexity of C-OPF guarantees that, even with mispredicted constraints, only one iteration of re-solving is necessary.

Our proposed approach presents significant advantages over other dual variable-based methods such as [26], [27]. First, our framework can handle nonlinear convex constraints, necessitating an analysis of the existence and uniqueness of the dual solution, as well as the validity of using dual variables for constraint classification. We provide the necessary analyses to support this. Second, previous methods lack provable robustness against mispredictions of dual variables and offer generalization guarantees that are difficult to quantify for practical C-OPF cases. We address this issue in the present paper. Finally, we develop a novel data augmentation technique to expedite the generation of synthetic data from existing datasets, enhancing MoGE training. Extensive simulations are performed on a variety of test cases from the PGLIB OPF library [28] to validate the merits of our proposed method.

Our main contributions are summarized as follows.

- We propose a CS method for accelerating C-OPF solvers, which leverages MoGE to learn the mapping from problem parameters to the optimal dual variables. Predicted dual solutions are used to identify non-binding constraints. If mispredictions are detected, C-OPF is resolved with an augmented list of constraints.
- We establish a model-agnostic condition for generic C-OPFs to verify the strong duality and uniqueness of the dual solution, which is essential for using dual variables to classify constraints at the optimum. This condition is confirmed to be valid for the widely used quadratic-convex relaxation of ACOPF.
- We present an efficient method for generating datasets to train MoGE, leveraging the convexity of C-OPF. Our method proves to be more effective than random sampling in the parameter space for bootstrapping existing datasets.

C. Organization and Notation

The paper is structured as follows. Section II introduces a standard form of C-OPF that encompasses various OPF models, with the quadratic-convex relaxation of ACOPF serving as a specific example. Section III begins with an exploration of the analytical properties of C-OPF. Subsequently, we establish theoretical results for QC-OPF concerning strong duality and the uniqueness of dual solutions. This section also details the design and training of MoGE, along with the data generation process. Section IV conducts simulations to comparatively analyze the proposed method against other CS approaches. The conclusion is presented in Section V, accompanied by key proofs provided in the Appendix.

Notation: Matrices and vectors are depicted in bold typeface. The n -dimensional real space is denoted by \mathbb{R}^n . $[n]$ denotes the set $\{1, \dots, n\}$. For a vector $\mathbf{a} \in \mathbb{R}^n$, a_i is its i^{th} element while $[\mathbf{a}]_{\mathcal{S}}$ denotes the subvector corresponding to a set $\mathcal{S} \subseteq [n]$. $|\mathcal{S}|$ is the cardinality of set \mathcal{S} . $\mathbf{a} \preceq \mathbf{b}$ denotes elementwise inequality between the two vectors, while (\mathbf{a}, \mathbf{b}) denotes their concatenation. $\nabla f(\mathbf{x})$ denote the gradient or Jacobian matrix of function $f(\mathbf{x})$ while $\nabla^2 f(\mathbf{x})$ is its Hessian. \mathbf{e}_i is the i^{th} canonical vector and \mathbf{I}_n is the $n \times n$ identity matrix. $\text{conv}\{\mathbf{x}_1, \dots, \mathbf{x}_n\} \triangleq \{\sum_{i=1}^n \alpha_i \mathbf{x}_i \mid \boldsymbol{\alpha} \succeq \mathbf{0}, \mathbf{1}^\top \boldsymbol{\alpha} = 1\}$

denotes the convex hull of a finite set $\{\mathbf{x}_i\}_{i=1}^n$. $j = \sqrt{-1}$ is the imaginary unit.

II. C-OPF AS PARAMETRIC CONVEX OPTIMIZATION

In this section, we represent C-OPF as a parametric convex optimization problem. This allows us to generate a well-defined mapping between problem parameters and optimal dual variables, which can then be used for CS. In general, constraints for any OPF problem can broadly be categorized into two types: the power flow equations and other operational constraints. The power flow model remains fixed across problem instances, while operational constraints, such as nodal power balance and line thermal limits, are designed to ensure the reliable operation of the power network. These constraints' bounds serve as problem parameters in our formulation.

A. Generic C-OPF Formulation

Concretely, we represent any C-OPF as the following parametric optimization problem:

$$\begin{aligned} \mathcal{V}(\boldsymbol{\gamma}, \boldsymbol{\xi}) &\triangleq \min_{\mathbf{x}} f(\mathbf{x}) & (1a) \\ \text{s.t. } &\mathbf{g}(\mathbf{x}) \preceq \mathbf{0}, \quad \mathbf{h}(\mathbf{x}) = \mathbf{0} & (1b) \\ &\tilde{\mathbf{g}}(\mathbf{x}) \preceq \boldsymbol{\gamma}, \quad \tilde{\mathbf{h}}(\mathbf{x}) = \boldsymbol{\xi} & (1c) \\ &\underline{\mathbf{x}} \preceq \mathbf{x} \preceq \bar{\mathbf{x}}. & (1d) \end{aligned}$$

Here, $\mathbf{x} \in \mathbb{R}^n$ is the decision variable whose exact description depends on the underlying power flow model. The convex objective function $f : \mathbb{R}^n \mapsto \mathbb{R}$ typically represents the total generation cost or power line loss over the network. Constraint functions $\mathbf{g} : \mathbb{R}^n \mapsto \mathbb{R}^L$ and $\mathbf{h} : \mathbb{R}^n \mapsto \mathbb{R}^M$ denote the power flow model, while $\tilde{\mathbf{g}} : \mathbb{R}^n \mapsto \mathbb{R}^{\tilde{L}}$ and $\tilde{\mathbf{h}} : \mathbb{R}^n \mapsto \mathbb{R}^{\tilde{M}}$ denote all other operational constraints.

The bounds for the operational constraints are captured by the right-hand side parameters $\boldsymbol{\gamma}$ and $\boldsymbol{\xi}$, which are used to parameterize the problem. For the parameter space, we consider open, nonempty subsets $\Gamma \subset \mathbb{R}^L$ and $\Xi \subset \mathbb{R}^M$ such that problem (1) is feasible for all $(\boldsymbol{\gamma}, \boldsymbol{\xi}) \in \Gamma \times \Xi$.

Definition 1. *The feasible power flow set is defined as*

$$\mathcal{X}_{\text{pf}} \triangleq \{\mathbf{x} : \mathbf{g}(\mathbf{x}) \preceq \mathbf{0}, \mathbf{h}(\mathbf{x}) = \mathbf{0}\}.$$

Definition 2. *The active set of the inequality constraint $\mathbf{g}(\mathbf{x}) \preceq \mathbf{0}$ at point \mathbf{x} is defined as*

$$\mathcal{A}_{\mathbf{g}}(\mathbf{x}) \triangleq \{i \in [L] : g_i(\mathbf{x}) = 0\}.$$

In the sequel, we show how the quadratic-convex relaxation to OPF (QC-OPF) [10] can be represented in the form of (1). QC relaxation is generally tighter than SOCP relaxation and faster to compute than SDP relaxation [9], [10]. While QC-OPF serves as our demonstrative example, the proposed framework and analysis are applicable to other C-OPF models.

TABLE I: Representing QC-OPF (2) as parametric convex optimization problem (1), where the box constraint (1d) corresponds to constraints (2g), (2h), and (2i).

Variables	Constraints	Parameters
\mathbf{x} : $\{P_k^g, Q_k^g\}_{k \in \mathcal{G}}$, $\{P_{ij}^g, Q_{ij}^g\}_{(i,j) \in \mathcal{E} \cup \mathcal{E}^R}$, $\{W_{ij}^R, W_{ij}^I\}_{(i,j) \in \mathcal{E}}, \{W_{ii}\}_{i \in \mathcal{N}}$	$g(\mathbf{x}), \tilde{g}(\mathbf{x})$: (2c)–(2d), (2f) $h(\mathbf{x}), \tilde{h}(\mathbf{x})$: (2b), (2e)	γ : $\{\bar{S}_{ij}\}_{(i,j) \in \mathcal{E}}, \{\bar{S}_{ij}\}_{(i,j) \in \mathcal{E}}$ ξ : $\{P_i^d, Q_i^d\}_{i \in \mathcal{N}}$

B. QC-OPF

QC-OPF is a convex relaxation to the ACOPF for meshed networks, possibly multiple generators on each bus, and transformers and phase shifters on each line. Let $(\mathcal{N}, \mathcal{E})$ denote the directed graph representing the power network, and \mathcal{E}^R the edges with the reversed orientation. Let $N = |\mathcal{N}|$ and $E = |\mathcal{E}|$ denote the total number of buses and power lines. Each bus $i \in \mathcal{N}$ is associated with the indices \mathcal{G}_i of generators attached to it, real and reactive demands P_i^d, Q_i^d , line charging admittance $g_i^s - j b_i^s$, and minimum (maximum) voltage magnitude \underline{V}_i (\bar{V}_i). In addition, the real and reactive power outputs of the k^{th} generator are denoted by P_k^g and Q_k^g , respectively. Set $\mathcal{G} \triangleq \cup_{i \in \mathcal{N}} \mathcal{G}_i$ collects all generation units. For each branch $(i, j) \in \mathcal{E}$, we have the thermal limit \bar{S}_{ij} , and the minimum and maximum phase angle differences (PAD) such that $-\frac{\pi}{2} < \underline{\theta}_{ij} < \bar{\theta}_{ij} < \frac{\pi}{2}$. Each branch is represented by a Π -model with the corresponding line matrix

$$\begin{bmatrix} y_{ij}^{\text{ff}} & y_{ij}^{\text{ft}} \\ y_{ij}^{\text{tf}} & y_{ij}^{\text{tt}} \end{bmatrix} \triangleq \begin{bmatrix} \left(y_{ij} + j \frac{b_{ij}^c}{2} \right) \frac{1}{|T_{ij}|^2} & -\frac{y_{ij}}{T_{ij}^*} \\ -\frac{y_{ij}}{T_{ij}} & y_{ij} + j \frac{b_{ij}^c}{2} \end{bmatrix},$$

where we have line admittance y_{ij} , total charging susceptance b_{ij}^c , and transformer parameter $T_{ij} = \tau_{ij} \angle \theta_{ij}^{\text{shift}}$.

Let V_i denote the voltage phasor at bus i and define $W_{ij} = W_{ij}^R + j W_{ij}^I \triangleq V_i V_j^*$. To this end, the QC-OPF formulation is given as follows.

$$\min \sum_{k \in \mathcal{G}} c_{k,2} (P_k^g)^2 + c_{k,1} P_k^g + c_{k,0} \quad (2a)$$

subject to:

$$\left. \begin{aligned} P_{ij} - \text{Re}(y_{ij}^{\text{ff}}) W_{ii} - \text{Re}(y_{ij}^{\text{ft}}) W_{ij}^R - \text{Im}(y_{ij}^{\text{ft}}) W_{ij}^I &= 0 \\ Q_{ij} - \text{Im}(y_{ij}^{\text{ff}}) W_{ii} - \text{Re}(y_{ij}^{\text{ft}}) W_{ij}^I + \text{Im}(y_{ij}^{\text{ft}}) W_{ij}^R &= 0 \\ P_{ji} - \text{Re}(y_{ij}^{\text{tf}}) W_{jj} - \text{Re}(y_{ij}^{\text{tt}}) W_{ij}^R + \text{Im}(y_{ij}^{\text{tt}}) W_{ij}^I &= 0 \\ Q_{ji} - \text{Im}(y_{ij}^{\text{tf}}) W_{jj} + \text{Re}(y_{ij}^{\text{tt}}) W_{ij}^I + \text{Im}(y_{ij}^{\text{tt}}) W_{ij}^R &= 0 \end{aligned} \right\} \quad (2b)$$

$$\forall (i, j) \in \mathcal{E} \quad (W_{ij}^R)^2 + (W_{ij}^I)^2 - W_{ii} W_{jj} \leq 0, \quad \forall (i, j) \in \mathcal{E} \quad (2c)$$

$$\tan(\underline{\theta}_{ij}) W_{ij}^R \leq W_{ij}^I \leq \tan(\bar{\theta}_{ij}) W_{ij}^R, \quad \forall (i, j) \in \mathcal{E} \quad (2d)$$

$$\left. \begin{aligned} \left(\sum_{k \in \mathcal{G}_i} P_k^g \right) - g_i^s W_{ii} - \sum_{(i,j) \in \mathcal{E} \cup \mathcal{E}^R} P_{ij} &= P_i^d \\ \left(\sum_{k \in \mathcal{G}_i} Q_k^g \right) + b_i^s W_{ii} - \sum_{(i,j) \in \mathcal{E} \cup \mathcal{E}^R} Q_{ij} &= Q_i^d \end{aligned} \right\}, \quad \forall i \in \mathcal{N} \quad (2e)$$

$$P_{ij}^2 + Q_{ij}^2 \leq \bar{S}_{ij}^2, \quad P_{ji}^2 + Q_{ji}^2 \leq \bar{S}_{ij}^2, \quad \forall (i, j) \in \mathcal{E} \quad (2f)$$

$$\underline{P}_k^g \leq P_k^g \leq \bar{P}_k^g, \quad \underline{Q}_k^g \leq Q_k^g \leq \bar{Q}_k^g, \quad \forall k \in \mathcal{G} \quad (2g)$$

$$\underline{V}_i^2 \leq W_{ii} \leq \bar{V}_i^2, \quad \forall i \in \mathcal{N} \quad (2h)$$

$$|W_{ij}^R| \leq \bar{V}_i \bar{V}_j, \quad |W_{ij}^I| \leq \bar{V}_i \bar{V}_j, \quad \forall (i, j) \in \mathcal{E}. \quad (2i)$$

In the above, the objective (2a) is a convex quadratic function of real power generation cost. (2b) describes the forward and reverse flows on each line, while (2c) denotes the SOCP relaxation of the cross-term dependence. (2d) enforces the PAD limits on each branch. (2e) represents the nodal power balance, while line flow constraints (2f) enforce the thermal limits. Finally, (2g), (2h), and (2i) represent the upper and lower bounds for the decision variables.

We can represent the QC-OPF (2) in the generic formulation (1), as shown in Table I. The parameterized inequality $\tilde{g}(\mathbf{x}) \leq \gamma$ contains the line flow constraints and the equality $\mathbf{h}(\mathbf{x}) = \xi$ contains the power balance equations. The latter is parameterized by real and reactive load demands, and the former by the line thermal limits.

III. CONSTRAINT SCREENING FOR C-OPF

We divide this section into two parts. The first part provides analysis for generalized C-OPF of the form (1). In the second part, we present the proposed accelerated solution based on constraint screening.

A. Analytical Properties of C-OPF

We start with a standard result of the value function $\mathcal{V}(\gamma, \xi)$.

Lemma 1 (Convexity of value function [29, pp. 250]). $\mathcal{V}(\gamma, \xi)$ is jointly convex in γ and ξ over any convex subset of $\Gamma \times \Xi$.

Corollary 1 (Feasibility in the parameter space). Assume problem (1) is feasible for each point in a finite set $\{(\gamma_k, \xi_k)\}_{k \in [K]}$. Then, the problem remains feasible for any point $(\tilde{\gamma}, \tilde{\xi}) \in \text{conv}\{(\gamma_1, \xi_1), \dots, (\gamma_K, \xi_K)\}$.

This corollary supports our data generation Algorithm 1, with a simple proof. $\mathcal{V}(\gamma_k, \xi_k)$ is finite because the problem is feasible for each point (γ_k, ξ_k) . Due to the convexity of \mathcal{V} , we have $\mathcal{V}(\tilde{\gamma}, \tilde{\xi}) \leq \sum_k \alpha_k \mathcal{V}(\gamma_k, \xi_k) < \infty$, where $\{\alpha_k\}$ are in the standard simplex. This confirms the problem is feasible for $(\tilde{\gamma}, \tilde{\xi})$.

Let $\lambda, \mu, \tilde{\lambda}, \tilde{\mu}$ denote the multipliers corresponding to the constraints (1b) and (1c). Then, the partial Lagrangian function of (1) can be written as

$$\begin{aligned} \mathcal{L}(\mathbf{x}, \lambda, \tilde{\lambda}, \mu, \tilde{\mu}) &\triangleq f(\mathbf{x}) + \lambda^\top \mathbf{g}(\mathbf{x}) + \mu^\top \mathbf{h}(\mathbf{x}) \\ &\quad + \tilde{\lambda}^\top (\tilde{\mathbf{g}}(\mathbf{x}) - \gamma) + \tilde{\mu}^\top (\tilde{\mathbf{h}}(\mathbf{x}) - \xi). \end{aligned}$$

The dual problem is

$$\sup_{\lambda \geq 0, \tilde{\lambda} \geq 0, \mu, \tilde{\mu}} D(\lambda, \tilde{\lambda}, \mu, \tilde{\mu}), \quad (3)$$

with the dual objective

$$\begin{aligned} D(\lambda, \tilde{\lambda}, \mu, \tilde{\mu}) &\triangleq \inf_{\mathbf{x} \preceq \mathbf{x} \preceq \bar{\mathbf{x}}} \mathcal{L}(\mathbf{x}, \lambda, \tilde{\lambda}, \mu, \tilde{\mu}) \\ &= -\tilde{\lambda}^\top \gamma - \tilde{\mu}^\top \xi + \inf_{\mathbf{x} \preceq \mathbf{x} \preceq \bar{\mathbf{x}}} \{f(\mathbf{x}) + \lambda^\top \mathbf{g}(\mathbf{x}) \\ &\quad + \mu^\top \mathbf{h}(\mathbf{x}) + \tilde{\lambda}^\top \tilde{\mathbf{g}}(\mathbf{x}) + \tilde{\mu}^\top \tilde{\mathbf{h}}(\mathbf{x})\}. \end{aligned} \quad (4)$$

If strong duality holds (meaning the optimal values of the primal and dual problems are equal), the structure in (4) indicates that (sub)gradients of $\mathcal{V}(\gamma, \xi)$ can be expressed as functions of the optimal dual solutions. Strong duality is not guaranteed in general, though it always holds for feasible linear programs [30, Chap. 6]. For convex problems, various results establish conditions under which strong duality holds. These conditions are called constraint qualifications (a.k.a. regularity conditions such as Slater's condition) [29, Section 5.2.3]. Constraint qualifications guarantee that a constrained minimizer satisfies the well-defined KKT system.

Next, we show that the special structure of QC-OPF (2) ensures strong duality by satisfying the *linear independence constraint qualification (LICQ)*.

Lemma 2 (Fixed LICQ). *Given QC-OPF (2), for all $\tilde{\mathbf{x}} \in \mathcal{X}_{\text{pf}}$ the LICQ holds with respect to constraints \mathbf{g} and \mathbf{h} , i.e., the Jacobian matrix of the binding constraints is full row rank¹:*

$$\text{rank} \left(\mathbf{J}(\tilde{\mathbf{x}}) \triangleq \begin{bmatrix} \nabla[\mathbf{g}(\tilde{\mathbf{x}})]_{\mathcal{A}_{\mathbf{g}}(\tilde{\mathbf{x}})} \\ \nabla \mathbf{h}(\tilde{\mathbf{x}}) \end{bmatrix} \right) = M + |\mathcal{A}_{\mathbf{g}}(\tilde{\mathbf{x}})|.$$

The proof is provided in Appendix A. This lemma allows us to extend LICQ to all constraints of QC-OPF over the entire parameter space. This is established in the following theorem.

Theorem 1 (Genericity of LICQ). *For every feasible point of QC-OPF (2) and for almost everywhere in the parameter space $\Gamma \times \Xi$, the LICQ holds with respect to all constraints $\mathbf{g}, \mathbf{h}, \tilde{\mathbf{g}}, \tilde{\mathbf{h}}$. Thus, strong duality holds for QC-OPF.*

The proof is provided in Appendix B. For the convex QC-OPF, strong duality implies $\mathcal{V}(\gamma, \xi) = -\tilde{\lambda}^{*\top} \gamma - \tilde{\mu}^{*\top} \xi + W$, where W denotes additional terms not involving γ or ξ (cf. (4)). Furthermore, LICQ ensures the existence and uniqueness of Lagrange multipliers satisfying the KKT system [31, Thm. 2]. Thus, the closed form of $\nabla_\gamma \mathcal{V}(\gamma, \xi)$ and $\nabla_\xi \mathcal{V}(\gamma, \xi)$ follows immediately, as given below.

Proposition 1 (Gradients of value function). *Given QC-OPF (2), for almost every $(\gamma, \xi) \in \Gamma \times \Xi$ we have*

$$\nabla_\gamma \mathcal{V}(\gamma, \xi) = -\tilde{\lambda}^*, \quad \nabla_\xi \mathcal{V}(\gamma, \xi) = -\tilde{\mu}^*, \quad (5)$$

where $\tilde{\lambda}^*$ and $\tilde{\mu}^*$ are the unique optimal solution to problem (3).

Since the optimal dual solution serves as the gradients of $\mathcal{V}(\gamma, \xi)$, we can develop a customized neural network to learn these gradients and predict binding constraints for CS, as demonstrated in subsection III-C. Note that the dual solution-based DCOPF solvers (e.g., [26]) can be considered as a special case of our framework.

¹For simplicity, full row rank is referred to as full rank hereinafter.

B. Strict Complementarity

In this part, we justify using dual variables to remove non-binding constraints at the optimum by assuming the following condition for C-OPF.

Assumption 1 (Strict complementarity). *Given C-OPF (1), the strict complementarity condition holds for $\tilde{\mathbf{g}}$, i.e., for any optimal primal-dual solution we have*

$$\tilde{\lambda}_i^* > 0, \text{ for all } i \in \mathcal{A}_{\tilde{\mathbf{g}}}(\mathbf{x}^*). \quad (6)$$

The strict complementarity condition asserts that all binding inequality constraints have strictly positive multipliers (i.e., no degenerate inequalities). As a standard assumption for interior-point method-based solvers [32], this condition always holds for feasible linear programs, which also applies to QC-OPF in our simulations. We will specifically focus on demonstrating how constraints in $\tilde{\mathbf{g}}(\mathbf{x}) \preceq \gamma$ can be eliminated using the knowledge of the optimal dual solution $\tilde{\lambda}^*$.

Proposition 2 (Constraint reduction equivalence). *Suppose it is known a priori that $\tilde{\lambda}_i^* = 0$ for $i \in \mathcal{J} \subseteq [\tilde{L}]$. Then, replacing constraint $\tilde{\mathbf{g}}(\mathbf{x}) \preceq \gamma$ in (1) with $[\tilde{\mathbf{g}}(\mathbf{x})]_{[\tilde{L}] \setminus \mathcal{J}} \preceq \gamma_{[\tilde{L}] \setminus \mathcal{J}}$ results in an equivalent problem.*

The proof is straightforward. Any optimal solution \mathbf{x}^* of the original problem satisfies the KKT system for the reduced problem, and vice versa. Consequently, the optimal solutions to both convex problems are identical. It is worth noting that Proposition 2 does not hold for nonconvex problems in general. Consider the problem

$$\min_{x \leq 0} (4x^2 + x + 1)(x^2 - 1),$$

where LICQ holds for all points. The KKT system is

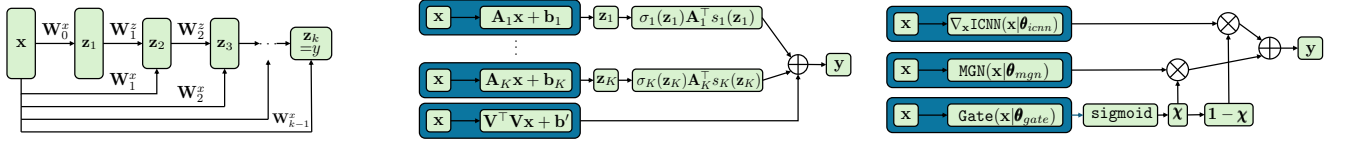
$$\begin{aligned} \nabla_x ((4x^2 + x + 1)(x^2 - 1) + \lambda x) &= 0 \\ x &\leq 0, \quad \lambda \geq 0, \quad \lambda x = 0. \end{aligned}$$

We can verify that $x^* = -0.6267, \lambda^* = 0$ is the globally optimal solution. Excluding the constraint $x \leq 0$ given $\lambda^* = 0$, the optimal solution to the unconstrained problem becomes $x^* = 0.6043$. Therefore, the reduced problem is not equivalent to the original one.

C. Constraint Screening via MoGE

In this section, we present the acceleration method for C-OPF by removing non-binding constraints from $\tilde{\mathbf{g}}(\mathbf{x}) \preceq \gamma$. Our strategy involves training a model which learns the gradients of $\mathcal{V}(\gamma, \xi)$, i.e. the mapping $(\gamma, \xi) \mapsto (-\tilde{\lambda}^*, -\tilde{\mu}^*)$ in supervised learning fashion. Then, a new problem instance is sped up by removing non-binding constraints identified from the predicted value of $\tilde{\lambda}^*$ using Assumption 1.

We aim to use machine learning models suitable for approximating gradients of convex functions, considering two possible approaches. The first approach, used by input convex neural networks (ICNNs) [33], approximates the scalar-valued mapping $(\gamma, \xi) \mapsto \mathcal{V}(\gamma, \xi)$. Gradients are then generated by calculating $\nabla \mathcal{V}$ using automatic differentiation (AD) during both training and inference. The second approach, utilized by



(a) $y = \text{ICNN}(\mathbf{x}|\theta_{icnn})$, with nonnegative weights $\{\mathbf{W}_i^z\}_{i=1}^{K-1}$ ensuring convexity of y in \mathbf{x} .

(b) $y = \text{MGN}(\mathbf{x}|\theta_{mgn})$, where $\{\sigma_i\}_{i=1}^K$ are convex, twice differentiable, nonnegative elementwise functions, and $\{s_i\}_{i=1}^K$ are their respective derivatives.

(c) MoGE architecture uses ICNN and MGN alongside a gating network Gate, which is used to soft-select the better output from the two experts.

Fig. 1: Schematic of the MoGE architecture, alongside its primary constituent elements ICNN and MGN.

monotone gradient networks (MGNs) [34], directly learns the mapping $(\gamma, \xi) \mapsto (-\tilde{\lambda}^*, -\tilde{\mu}^*)$ without using AD.

A K -layer ICNN, denoted as $y = \mathbf{z}_K = \text{ICNN}(\mathbf{x}|\theta_{icnn})$, uses the architecture

$$\mathbf{z}_{k+1} = \sigma_k(\mathbf{W}_k^z \mathbf{z}_k + \mathbf{W}_k^x \mathbf{x} + \mathbf{b}_k), \quad k = 0, \dots, K-1,$$

where \mathbf{z}_i denotes the layer activations with $\mathbf{z}_0 \equiv \mathbf{0}$ and $\mathbf{W}_0^z \equiv \mathbf{0}$. σ_i are non-linear activation functions and $\theta_{icnn} = \{\mathbf{W}_{0:K-1}^x, \mathbf{W}_{1:K-1}^z, \mathbf{b}_{0:K-1}\}$ are the learnable parameters. If all weights $\mathbf{W}_{1:K-1}^z$ are nonnegative and all functions σ_i are convex and non-decreasing, then ICNN is convex in its input-to-output mapping [33, Prop. 1]. Consequently, $\nabla_{\mathbf{x}} \text{ICNN}(\mathbf{x}|\theta_{icnn})$ can be used to learn the dual variables. On the other hand, MGN is a shallow architecture with K units given as

$$\begin{aligned} y &= \text{MGN}(\mathbf{x}|\theta_{mgn}) = \mathbf{b}' + \mathbf{V}^\top \mathbf{V} \mathbf{x} + \sum_{k=1}^K \sigma_k(\mathbf{z}_k) \mathbf{A}_k^\top s_k(\mathbf{z}_k), \\ \mathbf{z}_k &= \mathbf{A}_k \mathbf{x} + \mathbf{b}_k \quad \forall k \in [K], \quad \theta_{mgn} = \{\mathbf{A}_{1:K}, \mathbf{b}_{1:K}, \mathbf{V}, \mathbf{b}'\}. \end{aligned}$$

Given convex, nonnegative, and twice differentiable elementwise activations σ_k with s_k being σ_k 's elementwise derivative, it can be shown that the Jacobian of MGN is positive semi-definite [34, Prop. 2]. Therefore, MGN is suitable for directly learning the gradients of convex functions.

In Section IV, ablative testing will reveal limitations in the ability of either of these two models to effectively learn dual variables. To address this, we adopt a mixture-of-experts (MoE) architecture named MoGE (Mixture of Gradient Experts). This approach integrates the strengths of both models using an auxiliary gating network, aiming to enhance robustness and performance in learning dual variables. MoE architectures, pioneered over three decades ago [35], are increasingly favored for their capability to leverage diverse model strengths effectively. Recent applications in large language models like Mixtral [36] underscore their suitability for complex tasks requiring nuanced learning and adaptation.

Letting χ denote the elementwise sigmoid function, the overall output of MoGE is

$$\begin{aligned} y &= \chi(\text{Gate}(\mathbf{x}|\theta_{gate})) \text{ICNN}(\mathbf{x}|\theta_{icnn}) \\ &\quad + (1 - \chi(\text{Gate}(\mathbf{x}|\theta_{gate}))) \text{MGN}(\mathbf{x}|\theta_{mgn}). \end{aligned}$$

The training process involves pre-training ICNN and MGN for a certain number of epochs, followed by training Gate on the

Algorithm 1 Dataset Generation and Training MoGE

Input: Upper bound $(\bar{\gamma}, \bar{\xi})$ and lower bound $(\underline{\gamma}, \underline{\xi})$, number of initial samples K_1 , number of convex hull samples K_2

Output: Trained MoGE

- 1: $\mathcal{D} = \{\}, \mathcal{D}_1 = \{\}, \mathcal{D}_2 = \{\}$
- 2: **for** $i = 1$ to K_1 **do** ▷ Generate 1st dataset
- 3: Sample $(\gamma, \xi) \sim \text{Unif}((\underline{\gamma}, \underline{\xi}), (\bar{\gamma}, \bar{\xi}))$
- 4: Solve (1) with parameters (γ, ξ)
- 5: **if** (1) is infeasible for (γ, ξ) **then**, continue
- 6: **else**
- 7: Record inputs & outputs $\mathbf{d} \triangleq (\gamma, \xi, \tilde{\lambda}^*, \tilde{\mu}^*)$
- 8: $\mathcal{D}_1 = \mathcal{D}_1 \cup \{\mathbf{d}\}$
- 9: **end if**
- 10: **end for**
- 11: **for** $i = 1$ to K_2 **do** ▷ Generate 2nd dataset
- 12: Randomly generate a point $(\gamma, \xi) \in \text{conv}\{(\gamma_1, \xi_1), \dots, (\gamma_{|\mathcal{D}_1|}, \xi_{|\mathcal{D}_1|})\}$
- 13: Solve (1) with the parameters (γ, ξ)
- 14: Record inputs & outputs $\mathbf{d} \triangleq (\gamma, \xi, \tilde{\lambda}^*, \tilde{\mu}^*)$
- 15: $\mathcal{D}_2 = \mathcal{D}_2 \cup \{\mathbf{d}\}$
- 16: **end for**
- 17: $\mathcal{D} = \mathcal{D}_1 \cup \mathcal{D}_2$
- 18: Train MoGE using minibatch training on losses $\{l_i\}_{i \in [|\mathcal{D}|]}$
- 19: **return** MoGE

outputs of the trained experts for the same number of epochs. We consider the mean-square error loss for the i^{th} data sample

$$l_i \triangleq \left\| [\text{MoGE}(\gamma_i, \xi_i)]_{(\mathcal{J}_{\tilde{\lambda}}, \mathcal{J}_{\tilde{\mu}})} - (\tilde{\lambda}_i^*, \tilde{\mu}_i^*) \right\|_2^2, \quad (7)$$

where $(\mathcal{J}_{\tilde{\lambda}}, \mathcal{J}_{\tilde{\mu}})$ are indices corresponding to $\tilde{\lambda}^*$ and $\tilde{\mu}^*$. During the training of Gate, a weighing factor of $100N$ is used for loss indices that are ground truth binding, thereby allowing better learning of sparse binding constraints. The Gate network acts as a polling mechanism which soft-selects the response of the more accurate expert as the final response.

D. Dataset Generation and Training

The dataset generation and MoGE training process are highlighted in Algorithm 1. As seen in Table (I), the parameters (γ, ξ) contain values such as real and reactive load demands and line flow limits. To enhance the robustness of CS to newly encountered values of such parameters, we first create dataset \mathcal{D}_1 by uniformly sampling γ and ξ over the corresponding

Algorithm 2 Constraint Screening based Accelerated C-OPF**Input:** Trained MoGE, feasible parameters (γ, ξ) **Output:** Solution \mathbf{x}^* to C-OPF (1)

```

1:  $\tilde{\lambda}^* = [\text{MoGE}(\gamma, \xi)]_{\mathcal{J}_{\tilde{\lambda}}} \triangleright$  Predict optimal dual vars.
2:  $\mathcal{A}_{\text{bind}} = \{i : \tilde{\lambda}_i^* \neq 0\} \triangleright$  Set of binding constr.
3:  $\mathcal{A}_{\text{viol}} = \emptyset \triangleright$  Set of violated constr.
4: do
5:   Replace  $\tilde{g}(\mathbf{x}) \preceq \gamma$  in (1) with  $[\tilde{g}(\mathbf{x})]_{\mathcal{A}_{\text{bind}}} \preceq [\gamma]_{\mathcal{A}_{\text{bind}}}$ 
6:   Solve the reduced version of (1)
7:   Save the optimal solution  $\mathbf{x}^*$ 
8:   Update  $\mathcal{A}_{\text{viol}} = \{i : \tilde{g}_i(\mathbf{x}^*) > \gamma_i\}$ 
9:   Update  $\mathcal{A}_{\text{bind}} = \mathcal{A}_{\text{bind}} \cup \mathcal{A}_{\text{viol}}$ 
10: while  $\mathcal{A}_{\text{viol}} \neq \emptyset$ 
11: return  $\mathbf{x}^*$ 

```

intervals. Each parameter dimension is sampled independently. Then, problem (1) with the sampled parameters is solved with an optimizer that returns the optimal dual variables. The parameters (γ, ξ) and the optimal dual variables $\tilde{\lambda}^*, \tilde{\mu}^*$ are all added to \mathcal{D}_1 . If an input parameter causes an infeasible problem, it is ignored. Two points are noteworthy. First, the sampling process can be replaced with the use of historic datasets from solving prior C-OPF problems. Second, employing the aforementioned sampling approach for generating the entire dataset could lead to numerous sampled parameters being infeasible, causing a significant waste of time. Therefore, we utilize the following method to bootstrap the generation of additional feasible parameters.

We enhance training data for MoGE by generating convex combinations of parameters from \mathcal{D}_1 and storing the results in \mathcal{D}_2 , ensuring problem feasibility and accelerating data generation per Corollary 1. For \mathcal{D}_1 , P_i^d and Q_i^d are uniformly sampled 1000 times within 150% of their nominal values while keeping line flow limits constant, focusing on real and reactive load variations. Given the infeasibility of many samples in \mathcal{D}_1 , \mathcal{D}_2 restores the total number to 5,000. Combining \mathcal{D}_1 and \mathcal{D}_2 into a single dataset \mathcal{D} , each entry includes input pairs (γ, ξ) and corresponding outputs $(\tilde{\lambda}^*, \tilde{\mu}^*)$. The entire dataset \mathcal{D} is split into training and test sets, with the last 1,000 data points reserved for testing. Finally, we train MoGE using mini-batch supervised learning on the training part of \mathcal{D} .

E. Accelerated C-OPF with CS

Following the training of MoGE, we use it to accelerate C-OPF as detailed in Algorithm 2. Given a new instance of (γ, ξ) , MoGE predicts the value of $\tilde{\lambda}^*$. Based on Assumption 1, non-zero elements of $\tilde{\lambda}^*$ indicate the corresponding constraints must be binding. False positive mispredictions (classifying a non-binding constraint as binding) merely increase the reduced problem size without affecting the optimal solution. However, false negative mispredictions (classifying a binding constraint as non-binding) can alter the optimal solution. In such cases, Algorithm 2 adds the violated constraints to the binding constraints and re-solves C-OPF. The following result shows that only one such step is necessary for convex problems.

TABLE II: Number of elements in different cases from the PGLIB library.

Cases	Buses	Lines	Generators	Transformers
case118	118	186	54	11
case793	793	913	97	145
case1354	1354	1991	260	240
case2312	2312	3013	226	857
case4601	4601	7199	408	2054
case10000	10000	13139	2016	2374

Proposition 3. *After the first iteration of the do-while loop in Algorithm 2, $\mathcal{A}_{\text{bind}} \cup \mathcal{A}_{\text{viol}}$ corresponds to the indices of non-zero elements in the true values of $\tilde{\lambda}^*$. Therefore, the loop runs at most twice almost everywhere in the parameter space.*

Proposition 3 ensures that only one iteration of re-solving is required when MoGE mispredicts the binding constraints. The modified constraints $[\tilde{g}(\mathbf{x})]_{\mathcal{A}_{\text{bind}}} \preceq [\gamma]_{\mathcal{A}_{\text{bind}}}$ in Algorithm 2 can remove many non-binding constraints. Therefore, the resulting C-OPF solve time can be significantly reduced, as shown next. We conclude this section by noting that Algorithm 2 is compatible with CS methods beyond MoGE.

Remark 1 (Generality of Algorithm 2). *In Algorithm 2, the sole role of MoGE is to generate the optimal dual variable $\tilde{\lambda}^*$ for identifying binding constraints. Therefore, Algorithm 2 can be used with any alternative method capable of identifying binding constraints as a function of (γ, ξ) . Furthermore, Prop. 3 continues to hold for CS methods other than MoGE, since it is only based on the properties of the C-OPF (viz. convexity, Prop. 1 and Assumption 1).*

IV. SIMULATIONS

We test the dataset generation Algorithm 1 and the accelerating C-OPF in Algorithm 2, focusing on the QC-OPF model (2). We utilize the PGLIB library for our test cases, selecting six specific cases detailed in Table II. The library provides grid topology, line and transformer parameters, nominal load demands, line thermal limits, and PAD limits. Variability in parameters (γ, ξ) arises from perturbations around the prescribed nominal values of P_i^d and Q_i^d at each bus.

We utilize the Python implementation of the IPOPT solver, *cyipopt* [37], to solve optimization problems. This solver is augmented with customized code to ensure efficient solutions for QC-OPF. *cyipopt* provides optimal primal-dual solutions, with the dual solutions used for subsequent simulation aspects.

A. Speeding up QC-OPF in cyipopt

As a Python implementation of IPOPT, *cyipopt* lacks the speed advantages of Julia's JIT-compiled IPOPT implementations. Nevertheless, we can achieve comparable speed improvements in Python by pre-computing coefficients, as outlined here. All implementations of IPOPT solve the problem

$$\begin{aligned}
& \min_{\mathbf{x} \in \mathbb{R}^n} F(\mathbf{x}) \\
& \text{s.t. } \underline{\ell} \preceq \ell(\mathbf{x}) \preceq \bar{\ell}, \quad \underline{\mathbf{x}} \preceq \mathbf{x} \preceq \bar{\mathbf{x}}
\end{aligned}$$

wherein $\ell : \mathbb{R}^n \mapsto \mathbb{R}^p$ are the lumped constraint functions, with equality constraints modeled by setting $\underline{\ell}_i = \bar{\ell}_i$. Given

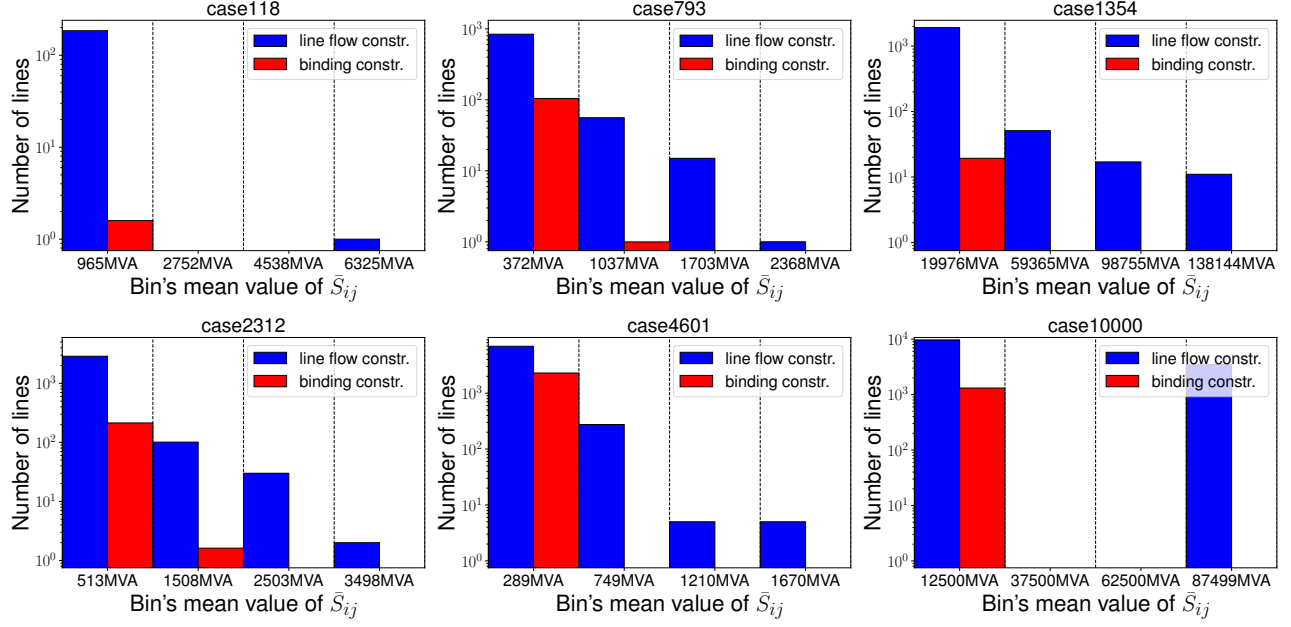


Fig. 2: Histograms of thermal limits, along with the average number (across the test set and forward/reverse flows) of corresponding line flow constraints which bind for different cases.

$\mathbf{x} \in \mathbb{R}^n$, $\boldsymbol{\alpha} \in \mathbb{R}^p$, and $\beta \in \mathbb{R}$, the user is required to provide routines that numerically compute the quantities $F(\mathbf{x})$, $\ell(\mathbf{x})$, $\nabla F(\mathbf{x})$, $\nabla \ell(\mathbf{x})$, and $\mathbf{H} := \beta \nabla^2 F(\mathbf{x}) + \sum_{j=1}^p \alpha_j \nabla^2 \ell_j(\mathbf{x})$. For QC-OPF, \mathbf{H} is linear in $(\beta, \boldsymbol{\alpha})$ and independent of \mathbf{x} while all other quantities are either linear or quadratic in \mathbf{x} . By pre-computing the coefficients of those terms, we achieve significant speedups since the computation of the above quantities reduces to sparse matrix-vector multiplications. For example, our implementation solves PGLIB case10000 in 50 seconds without any constraint removal, compared to 67 seconds for the Julia-based IPOPT package *PowerModels.jl* [38], despite lacking Julia's JIT features.

Furthermore, quadratic line flow constraints (2f) add significant computation overhead due to their contribution of linear terms to $\nabla \ell(\mathbf{x})$ and constant terms to $\sum_{j=1}^p \alpha_j \nabla^2 \ell_j(\mathbf{x})$. However, most of these constraints are not binding at the optimum, as shown in Figure 2. Therefore, enhancing the speed of any CS algorithm involves accurately detecting and removing non-binding line flow constraints, which are part of the constraints $\tilde{\mathbf{g}}(\mathbf{x}) \preceq \boldsymbol{\gamma}$ in our model.

B. CS Classifiers

Our design of MoGE involves ICNN with $K = 5$ and layer sizes $(2N + 2E, N + E, 300, 150, 2N + 2E)$, and LeakyReLU activations with slope 0.1 for negative values of x . MGN is chosen with $K = 2$, σ_k is chosen as LeakyReLU and Softplus, and $\mathbf{V}^\top \mathbf{V}$ is chosen to have rank 200 for all cases. Gate is a 2-layer network with a hidden layer of size 100, and LeakyReLU activation. The Adam optimizer is used to train MoGE for 2000 epochs with a batch size of 64. Once MoGE has been trained via Algorithm 1, 100 randomly selected examples from the test set are fed in Algorithm 2 to observe the acceleration of C-OPF. We train MoGE via PyTorch, which is carried out on a

system with an Intel Core i9 processor, 64 GB of RAM, and two NVIDIA RTX 3090 GPUs.

We can compare the proposed MoGE-based approach with other benchmark classification methods:

- To conduct an ablation study of MoGE, we list the performance of standalone ICNN and MGN. The former is a state-of-the-art architecture for learning dual variables in convex problems; see [39].
- *Deep classifier* is an DNN, which takes $(\boldsymbol{\gamma}, \boldsymbol{\xi})$ as input and produces \tilde{L} scalars in the range $(0, 1)$ as output, representing the probability of each of the \tilde{L} constraints binding [40]. We employ a 4-layer DNN with same layer sizes as the MoGE, and train it on dataset \mathcal{D} using binary cross-entropy loss. Training is performed for 2,000 epochs using the Adam optimizer with a batch size of 64.
- *Ridge classifier* uses PyTorch to train a ridge regression classifier on \mathcal{D}_1 . It first converts the targets (indicating binding and non-binding constraints) to $\{-1, 1\}$, then fits a linear model that maps the input parameters to these targets using ridge regression.
- *XGBoost classifier* involves training a gradient-boosted decision-tree classifier. The XGBoost package is used with a tree depth of 4, trained for 50 epochs at a learning rate of 0.1.

C. Numerical Results

All classifiers' predictions are fed into Algorithm 2. The comparative results are presented in Table III, including the training time, confusion matrix, total solve times, and the fraction of cases requiring resolution due to the detection of violated constraints.

Deep and ridge classifiers, along with MGN, train the fastest, whereas MoGE takes longer due to its MoE-based framework.

TABLE III: Performance evaluation of constraint classification approaches based on average solve time, training time, and fraction of re-solves for 50 test samples.

Method of Constr. Removal	Training Time	Confusion Matrix (Full Test Set)				Average Solve Time (100 samples)	Percent Reduction in Solve Time	Fraction Resolved (100 samples)
		True Positive	True Negative	False Positive	False Negative			
case118								
Original problem	-	0.86%	99.14%	-	-	0.1340s	-	-
MoGE	42.9275s	0.86%	94.35%	4.79%	0.00%	0.1045s	22.01%	0.00
ICNN	17.7126s	0.83%	95.68%	3.47%	0.02%	0.1043s	22.16%	0.00
MGN	2.1961s	0.83%	4.88%	94.26%	0.02%	0.1255s	-32.23%	0.00
Deep classifier	3.7815s	0.51%	99.12%	0.02%	0.34%	0.1772s	-27.61%	0.69
Ridge regression	3.3604s	0.52%	99.10%	0.04%	0.33%	0.1710s	-32.46%	0.63
XGBoost	1.5327s	0.51%	99.12%	0.03%	0.34%	0.1775s	-38.39%	0.70
case793								
Original problem	-	11.55%	88.45%	-	-	1.4356s	-	-
MoGE	19.5617s	11.55%	52.42%	36.03%	2e-4%	1.2295s	14.35%	0.00
ICNN	10.3576s	6.02%	82.91%	5.53%	5.53%	1.0543s	26.56%	0.01
MGN	4.8750s	11.43%	2.46%	85.99%	0.12%	1.3721s	4.42%	0.00
Deep classifier	5.4422s	11.13%	79.48%	8.96%	0.42%	2.0359s	-41.81%	0.88
Ridge regression	4.8871s	11.32%	79.23%	9.22%	0.24%	2.0152s	-40.37%	0.87
XGBoost	17.1395s	9.57%	81.01%	7.44%	1.99%	2.0153s	-40.38%	0.89
case1354								
Original problem	-	0.97%	99.03%	-	-	4.8173s	-	-
MoGE	28.1495s	0.97%	97.24%	1.79%	4e-5%	3.1845s	33.89%	0.00
ICNN	12.8741s	0.97%	97.64%	1.39%	6e-4%	3.4660s	28.46%	0.09
MGN	11.4738s	0.95%	3.24%	95.79%	0.02%	4.9438s	-2.62%	0.10
Deep classifier	7.5701s	0.92%	98.99%	0.04%	0.05%	4.9895s	-3.57%	0.60
Ridge regression	6.4307s	0.92%	98.99%	0.04%	0.05%	4.9814s	-3.40%	0.60
XGBoost	33.3336s	0.90%	99.01%	0.02%	0.07%	6.0771s	-26.15%	0.97
case2312								
Original problem	-	7.14%	92.86%	-	-	8.2118s	-	-
MoGE	49.6899s	7.13%	87.17%	5.69%	3e-4%	6.1273s	25.38%	0.00
ICNN	16.6255s	7.07%	89.91%	2.96%	0.07%	6.3821s	22.28%	0.06
MGN	25.6937s	7.12%	0.45%	92.42%	0.02%	6.9805s	14.99%	0.00
Deep classifier	11.0422s	6.92%	92.62%	0.25%	0.21%	11.8886s	-44.77%	1.00
Ridge regression	12.9950s	7.04%	91.57%	1.30%	0.09%	11.4918s	-39.94%	0.92
XGBoost	90.4948s	6.85%	92.67%	0.19%	0.29%	11.9112s	-45.04%	1.00
case4601								
Original problem	-	31.93%	68.07%	-	-	21.5637s	-	-
MoGE	171.3697s	31.93%	58.49%	9.57%	0.00%	17.2174s	20.15%	0.00
ICNN	26.6654s	31.76%	59.28%	8.79%	0.17%	17.3095s	19.72%	0.00
MGN	101.7099s	31.87%	3.22%	64.85%	0.06%	19.6766s	18.02%	0.00
Deep classifier	21.4779s	31.91%	59.24%	8.83%	0.02%	17.4671s	18.99%	0.03
Ridge regression	40.9736s	31.91%	59.24%	8.83%	0.02%	17.4176s	19.22%	0.03
XGBoost	569.9688s	31.76%	59.32%	8.75%	0.17%	17.4676s	18.99%	0.03
case10000								
Original problem	-	9.94%	90.06%	-	-	49.5253s	-	-
MoGE	580.2680s	9.94%	86.99%	3.07%	0.00%	38.8593s	21.53%	0.00
ICNN	48.1584s	8.87%	87.61%	2.44%	1.07%	39.5128s	20.21%	0.02
MGN	363.8684s	9.94%	26.54%	63.52%	0.00%	44.1753s	8.76%	0.00
Deep classifier	72.0453s	9.93%	87.31%	2.75%	0.01%	45.1290s	8.78%	0.17
Ridge regression	197.7062s	9.93%	87.31%	2.75%	0.01%	45.1855s	8.76%	0.17
XGBoost	-OOT-	-	-	-	-	-	-	-

However, MoGE's training time scales well with the number of buses, unlike XGBoost, which becomes impractical for larger cases. For example, XGBoost training for case10000 exceeds 12 hours and fails to complete.

The proposed MoGE-based CS method shows high true positives and low false negatives but has relatively lower true negatives and higher false positives. This outcome is acceptable because, in constraint classification, minimizing false negatives is critical to avoid constraint violations in the reduced problem, which would require re-solving and significantly increase the total runtime of Algorithm 2. The MoGE achieves very low false negatives, helping to avoid re-solves and resulting in the lowest solve times in most cases.

Additionally, MoGE achieves lower false negatives than ICNN and MGN, which is beneficial for larger cases. Interestingly, MGN tends to classify most constraints as binding, allowing Gate to switch to MGN if ICNN makes a false positive error.

The solve time advantage of MoGE ranges from 20% to 35%, which is significant when C-OPF needs to be solved repeatedly or when computational resources are limited. While ICNN performs similarly, MoGE is more robust in avoiding re-solves. Additionally, although the deep classifier and XGBoost offer good classification performance, they cannot match the efficiency of architectures like MoGE and ICNN designed to approximate convex functions and their gradients.

V. CONCLUSION

In this paper, we introduced a data-driven constraint screening approach to expedite convexified optimal power flow, utilizing the architecture of monotone neural networks. We presented a general technique based on rank conditions to assess the suitability of a given convexified OPF model for acceleration and explored methods for dataset generation and augmentation across OPF parameters. Numerical simulations illustrate that the proposed method significantly reduces the solve times for large-scale OPF problems while provably ensuring the same solution as the unreduced problem. Future research directions include incorporating switching topology, such as line connectivity and parameters into the accelerator. Additionally, we aim to leverage duality theory techniques employed in this work to accelerate distributed OPF in a data-driven manner.

REFERENCES

- [1] W. A. Bukhsh, A. Grothey, K. I. M. McKinnon, and P. A. Trodden, "Local solutions of the optimal power flow problem," *IEEE Trans. Power Syst.*, vol. 28, no. 4, pp. 4780–4788, 2013.
- [2] A. J. Wood, B. F. Wollenberg, and G. B. Sheblé, *Power generation, operation, and control*. John Wiley & Sons, 2013.
- [3] R. A. Jabr, "Radial distribution load flow using conic programming," *IEEE Trans. Power Syst.*, vol. 21, no. 3, pp. 1458–1459, 2006.
- [4] M. Farivar, C. R. Clarke, S. H. Low, and K. M. Chandy, "Inverter VAR control for distribution systems with renewables," in *2011 IEEE Intl Conf. on Smart Grid Commun.*, pp. 457–462.
- [5] M. Farivar and S. H. Low, "Branch flow model: Relaxations and convexification—part I," *IEEE Trans. Power Syst.*, vol. 28, no. 3, pp. 2554–2564, 2013.
- [6] X. Bai, H. Wei, K. Fujisawa, and Y. Wang, "Semidefinite programming for optimal power flow problems," *International Journal of Electrical Power & Energy Systems*, vol. 30, no. 6–7, pp. 383–392, 2008.
- [7] R. Madani, S. Sojoudi, and J. Lavaei, "Convex relaxation for optimal power flow problem: Mesh networks," *IEEE Trans. Power Syst.*, vol. 30, no. 1, pp. 199–211, 2015.
- [8] J. Lavaei and S. H. Low, "Zero duality gap in optimal power flow problem," *IEEE Trans. Power Syst.*, vol. 27, no. 1, pp. 92–107, 2012.
- [9] S. Bose, S. H. Low, T. Teeraratkul, and B. Hassibi, "Equivalent relaxations of optimal power flow," *IEEE Transactions on Automatic Control*, vol. 60, no. 3, pp. 729–742, 2015.
- [10] C. Coffrin, H. L. Hijazi, and P. Van Hentenryck, "The QC relaxation: A theoretical and computational study on optimal power flow," *IEEE Transactions on Power Systems*, vol. 31, no. 4, pp. 3008–3018, 2016.
- [11] B. Kocuk, S. S. Dey, and X. A. Sun, "Strong SOCP relaxations for the optimal power flow problem," *Operations Research*, vol. 64, no. 6, pp. 1177–1196, 2016.
- [12] D. K. Molzahn and I. A. Hiskens, "A survey of relaxations and approximations of the power flow equations," *Foundations and Trends® in Electric Energy Systems*, vol. 4, no. 1–2, pp. 1–221, 2019.
- [13] J. Telgen, "Identifying redundant constraints and implicit equalities in systems of linear constraints," *Management Science*, vol. 29, no. 10, pp. 1209–1222, 1983.
- [14] G. L. Thompson, F. M. Tonge, and S. Zions, "Techniques for removing nonbinding constraints and extraneous variables from linear programming problems," *Manag. Sci.*, vol. 12, no. 7, pp. 588–608, 1966.
- [15] Z. J. Zhang, P. T. Mana, D. Yan, Y. Sun, and D. K. Molzahn, "Study of active line flow constraints in DC optimal power flow problems," in *2020 SoutheastCon*, 2020, pp. 1–8.
- [16] B. Hua, Z. Bie, C. Liu, G. Li, and X. Wang, "Eliminating redundant line flow constraints in composite system reliability evaluation," *IEEE Trans. Power Syst.*, vol. 28, no. 3, pp. 3490–3498, 2013.
- [17] R. Weinhold and R. Mieth, "Fast security-constrained optimal power flow through low-impact and redundancy screening," *IEEE Trans. Power Syst.*, vol. 35, no. 6, pp. 4574–4584, 2020.
- [18] R. Madani, J. Lavaei, and R. Baldick, "Constraint screening for security analysis of power networks," *IEEE Trans. Power Syst.*, vol. 32, no. 3, pp. 1828–1838, 2017.
- [19] S. Pineda, J. M. Morales, and A. Jiménez-Cordero, "Data-driven screening of network constraints for unit commitment," *IEEE Trans. Power Syst.*, vol. 35, no. 5, pp. 3695–3705, 2020.
- [20] S. Zhang, H. Ye, F. Wang, Y. Chen, S. Rose, and Y. Ma, "Data-aided offline and online screening for security constraint," *IEEE Trans. Power Syst.*, vol. 36, no. 3, pp. 2614–2622, 2021.
- [21] A. Porras, S. Pineda, J. M. Morales, and A. Jiménez-Cordero, "Cost-driven screening of network constraints for the unit commitment problem," *IEEE Trans. Power Syst.*, vol. 38, no. 1, pp. 42–51, 2023.
- [22] D. Deka and S. Misra, "Learning for DC-OPF: Classifying active sets using neural nets," in *2019 IEEE Milan PowerTech*, 2019, pp. 1–6.
- [23] F. Hasan and A. Kargarian, "Topology-aware learning assisted branch and ramp constraints screening for dynamic economic dispatch," *IEEE Trans. Power Syst.*, vol. 37, no. 5, pp. 3495–3505, 2022.
- [24] F. Fioretto, T. W. Mak, and P. Van Hentenryck, "Predicting AC optimal power flows: Combining deep learning and lagrangian dual methods," *Proceedings of the AAAI Conference on Artificial Intelligence*, vol. 34, no. 01, pp. 630–637, Apr. 2020.
- [25] M. K. Singh, V. Kekatos, and G. B. Giannakis, "Learning to solve the AC-OPF using sensitivity-informed deep neural networks," *IEEE Trans. Power Syst.*, vol. 37, no. 4, pp. 2833–2846, 2022.
- [26] L. Zhang, Y. Chen, and B. Zhang, "A convex neural network solver for DCOF with generalization guarantees," *IEEE Trans. on Control of Network Syst.*, vol. 9, no. 2, pp. 719–730, 2022.
- [27] R. Nellikkath and S. Chatzivasileiadis, "Physics-informed neural networks for AC optimal power flow," *Electric Power Systems Research*, vol. 212, p. 108412, 2022.
- [28] S. Babaeinejad-sarookolae, A. Birchfield, R. Christie, C. Coffrin *et al.*, "The power grid library for benchmarking AC optimal power flow algorithms," *arXiv preprint arXiv:1908.02788*, 2019.
- [29] S. Boyd and L. Vandenberghe, *Convex optimization*. Cambridge University Press, 2004.
- [30] J. Matouek and B. Gärtner, *Understanding and Using Linear Programming*. Springer, 2006.
- [31] G. Wachsmuth, "On LICQ and the uniqueness of Lagrange multipliers," *Operations Research Letters*, vol. 41, no. 1, pp. 78–80, 2013.
- [32] A. Forsgren, P. E. Gill, and M. H. Wright, "Interior methods for nonlinear optimization," *SIAM review*, vol. 44, no. 4, pp. 525–597, 2002.
- [33] B. Amos, L. Xu, and J. Z. Kolter, "Input convex neural networks," in *Proceedings of the 34th Intl. Conf. on Machine Learning*, ser. Proceedings of Machine Learning Research, D. Precup and Y. W. Teh, Eds., vol. 70. PMLR, 06–11 Aug 2017, pp. 146–155.
- [34] S. Chaudhari, S. Pranav, and J. M. Moura, "Learning gradients of convex functions with monotone gradient networks," in *2023 IEEE Intl. Conf. on Acoustics, Speech and Signal Processing (ICASSP)*, 2023, pp. 1–5.
- [35] R. Jacobs, M. Jordan, S. Nowlan, and G. Hinton, "Adaptive mixtures of local experts," *Neural Computation*, vol. 3, no. 1, pp. 79–87, 1991.
- [36] A. Jiang, A. Sablayrolles, A. Roux, A. Mensch *et al.*, "Mixtral of experts," *arXiv preprint arXiv:2401.04088*, 2024.
- [37] A. Wächter and L. T. Biegler, "On the implementation of an interior-point filter line-search algorithm for large-scale nonlinear programming," *Mathematical programming*, vol. 106, pp. 25–57, 2006.
- [38] C. Coffrin, R. Bent, K. Sundar, Y. Ng, and M. Lubin, "Powermodels.jl: An open-source framework for exploring power flow formulations," in *2018 Power Syst. Computation Conf. (PSCC)*. IEEE, 2018, pp. 1–8.
- [39] Y. Chen, L. Zhang, and B. Zhang, "Learning to solve DCOF: A duality approach," *Electric Power Systems Research*, vol. 213, p. 108595, 2022.
- [40] D. Deka and S. Misra, "Learning for DC-OPF: Classifying active sets using neural nets," in *2019 IEEE Milan PowerTech*, pp. 1–6.
- [41] R. Horn and C. Johnson, *Matrix analysis*, 2nd ed. Cambridge University Press, 2012.
- [42] A. Hauswirth, S. Bolognani, G. Hug, and F. Dörfler, "Generic existence of unique Lagrange multipliers in AC optimal power flow," *IEEE Control Systems Letters*, vol. 2, no. 4, pp. 791–796, 2018.
- [43] J. Borwein and A. Lewis, *Convex Analysis and Nonlinear Optimization: Theory and Examples*, 2nd ed. Springer, 2006.

APPENDIX

A. Proof of Lemma 2

Let $\mathcal{A}_g(\mathbf{x}) = \mathcal{A}_{\text{soc}}(\mathbf{x}) \cup \mathcal{A}_{\text{ang}}(\mathbf{x})$, where $\mathcal{A}_{\text{soc}}(\mathbf{x})$ is the set of SOC binding constraints in (2c). $\mathcal{A}_{\text{ang}}(\mathbf{x}) \triangleq \mathcal{A}_{\text{ang}}^{\text{low}}(\mathbf{x}) \cup \mathcal{A}_{\text{ang}}^{\text{up}}(\mathbf{x})$ is the set of angle binding constraints in (2d), which reflects

the bindings at the PAD lower or upper limits.² Also, Let $l(m) : [E] \mapsto \mathcal{E}$ be the function mapping each index in $[E]$ to a unique line in \mathcal{E} . Define the partial set of variables $\mathbf{x}_s \triangleq \{P_{ij}, Q_{ij}, P_{ji}, Q_{ji}, W_{ij}^R, W_{ij}^I\}_{(i,j) \in \mathcal{E}}$. Let \mathbf{J}_s be the submatrix of the Jacobian \mathbf{J} formed by the columns corresponding to \mathbf{x}_s . We can compactly express it as a block upper triangular matrix of size $(4E + |\mathcal{A}_g(\mathbf{x})|) \times 6E$, as follows:

$$\mathbf{J}_s = \begin{array}{c} (2b) \\ (2c) \\ (2d) \end{array} \begin{pmatrix} P_{ij} & Q_{ij} & P_{ji} & Q_{ji} & W_{ij}^R & W_{ij}^I \\ & \mathbf{I}_{4E} & & & & * \\ \hline & \mathbf{0} & & & \underbrace{\begin{bmatrix} \mathbf{S}^R & \mathbf{S}^I \\ \mathbf{A}^R & \mathbf{A}^I \end{bmatrix}}_{\mathbf{J}_g} \end{pmatrix}$$

where the four submatrices are given as:

$$\begin{aligned} \mathbf{S}^R &= [2W_{l(m)}^R \mathbf{e}_m^\top : m \in \mathcal{A}_{\text{soc}}] \\ \mathbf{S}^I &= [2W_{l(m)}^I \mathbf{e}_m^\top : m \in \mathcal{A}_{\text{soc}}] \\ \mathbf{A}^R &= \begin{cases} \tan(\theta_{l(m)}) \mathbf{e}_m^\top & \text{if } m \in \mathcal{A}_{\text{ang}}^{\text{low}} \\ -\tan(\theta_{l(m)}) \mathbf{e}_m^\top & \text{if } m \in \mathcal{A}_{\text{ang}}^{\text{up}} \end{cases} \\ \mathbf{A}^I &= \begin{cases} -\mathbf{e}_m^\top & \text{if } m \in \mathcal{A}_{\text{ang}}^{\text{low}} \\ \mathbf{e}_m^\top & \text{if } m \in \mathcal{A}_{\text{ang}}^{\text{up}} \end{cases}. \end{aligned}$$

Note that these submatrices are constructed row by row using scaled canonical vectors $\{\mathbf{e}_m^\top\}$, with scaling factors determined by specific conditions. Furthermore, we have $W_{l(m)}^R \neq 0, \forall m \in \mathcal{A}_{\text{soc}}(\mathbf{x})$. Otherwise, $W_{l(m)}^I = 0$ due to (2d), which implies $W_{ii} = 0$ for some i (cf. binding constraint (2c)). This would violate the box constraint (2h) with nonzero \underline{V}_i^2 .

We will explore the special structure of $\mathbf{J}_g(\mathbf{x})$ to demonstrate its full rank for any $\mathbf{x} \in \mathcal{X}_{\text{pf}}$, thereby establishing the full rank of \mathbf{J}_s and \mathbf{J} [41, Sec. 0.9.4]. First, if $\mathcal{A}_g = \emptyset$, then $\mathbf{J}_s = [\mathbf{I}_{4E} \quad *]$, which is full rank. Otherwise, depending on the binding possibilities of (2c) and (2d), we have four cases: i) $\mathcal{A}_{\text{soc}} = \emptyset, \mathcal{A}_{\text{ang}} \neq \emptyset$; ii) $\mathcal{A}_{\text{soc}} \neq \emptyset, \mathcal{A}_{\text{ang}} = \emptyset$; iii) $\mathcal{A}_{\text{soc}} \neq \emptyset, \mathcal{A}_{\text{ang}} \neq \emptyset, \mathcal{A}_{\text{soc}} \cap \mathcal{A}_{\text{ang}} = \emptyset$; and iv) $\mathcal{A}_{\text{soc}} \cap \mathcal{A}_{\text{ang}} \neq \emptyset$. In each of the first three cases, \mathbf{J}_g is full rank as it is in *row echelon form (REF) without zero rows*, possibly after row permutations.

Finally, the most complex case-iv occurs when both the SoC constraint and one of the angle limit constraints are simultaneously binding for at least one line. Define $\rho_m \triangleq \frac{-\tan(\theta_{l(m)})}{2W_{l(m)}^R}, \forall m \in \mathcal{A}_{\text{soc}} \cap \mathcal{A}_{\text{ang}}^{\text{low}}$. For each m , the two corresponding rows in \mathbf{J}_g have only four nonzero elements. Applying the elementary row operation:

$$\begin{bmatrix} \cdots & 2W_{l(m)}^R & \cdots & 2W_{l(m)}^I & \cdots \\ \cdots & \tan(\theta_{l(m)}) & \cdots & -1 & \cdots \end{bmatrix} \xrightarrow{r_2 + \rho_m \times r_1} \begin{bmatrix} \cdots & 2W_{l(m)}^R & \cdots & 2W_{l(m)}^I & \cdots \\ \cdots & 0 & \cdots & p & \cdots \end{bmatrix},$$

we get the pivot $p = -(1 + \tan^2(\theta_{l(m)})) \neq 0$ for the second row. Similarly, define $\tilde{\rho}_m \triangleq \frac{\tan(\theta_{l(m)})}{2W_{l(m)}^R}, \forall m \in \mathcal{A}_{\text{soc}} \cap \mathcal{A}_{\text{ang}}^{\text{up}}$, we get the pivot $\tilde{p} = 1 + \tan^2(\theta_{l(m)}) \neq 0$ with the same row

operation. By repeating the aforementioned operation for all $m \in \mathcal{A}_{\text{soc}} \cap \mathcal{A}_{\text{ang}}$, we convert \mathbf{J}_g into *REF without zero rows*, confirming its full rank.

B. Proof of Theorem 1

Consider the following parametric (not necessarily convex) problem, where the parameter space Θ is an open, nonempty set with non-zero measure.

$$\begin{aligned} \mathcal{P}(\boldsymbol{\theta}) &\triangleq \min_{\mathbf{x} \in \mathbb{R}^n} f(\mathbf{x}) \\ \text{s.t.} \quad &\mathbf{g}(\mathbf{x}) \preceq \mathbf{0}, \quad \mathbf{h}(\mathbf{x}) = \mathbf{0} \\ &\tilde{\mathbf{g}}(\mathbf{x}, \boldsymbol{\theta}) \preceq \mathbf{0}, \quad \tilde{\mathbf{h}}(\mathbf{x}, \boldsymbol{\theta}) = \mathbf{0}. \end{aligned}$$

Theorem (Genericity of LICQ [42]). *Consider the problem $\mathcal{P}(\boldsymbol{\theta})$ with $f, \mathbf{g}, \mathbf{h}, \tilde{\mathbf{g}}, \tilde{\mathbf{h}}$ in class C^r (i.e., r -times continuously differentiable) for all $\mathbf{x} \in \mathcal{X}_{\text{pf}}$ and $\boldsymbol{\theta} \in \Theta$ with $r > \max(0, n - M - \tilde{M})$ and assume LICQ holds for all $\mathbf{x} \in \mathcal{X}_{\text{pf}}$. If the map $\boldsymbol{\theta} \mapsto (\tilde{\mathbf{g}}(\mathbf{x}, \boldsymbol{\theta}), \tilde{\mathbf{h}}(\mathbf{x}, \boldsymbol{\theta}))$ has rank $\tilde{M} + \tilde{L}$ for every $\mathbf{x} \in \mathcal{X}_{\text{pf}}$ and $\boldsymbol{\theta} \in \Theta$, then LICQ holds for almost every $\boldsymbol{\theta} \in \Theta$ and for every feasible point of $\mathcal{P}(\boldsymbol{\theta})$.*

To prove Theorem 1, we will demonstrate that QC-OPF satisfies all conditions stated in the theorem above. That is, C1) all functions are in class C^r ; C2) the parameter-to-constraint map is full rank; and C3) LICQ holds for all $\mathbf{x} \in \mathcal{X}_{\text{pf}}$, which is already established in Lemma 2. First, since all functions in QC-OPF are either affine or quadratic, they are infinitely differentiable, thereby satisfying condition C1). Second, let us consider embedding the box constraint $\underline{\mathbf{x}} \preceq \mathbf{x} \preceq \bar{\mathbf{x}}$ into $\tilde{\mathbf{g}}$. The parameter-to-constraint map of C-OPF is $(\boldsymbol{\gamma}, \boldsymbol{\xi}) \mapsto (\tilde{\mathbf{g}}(\mathbf{x}) - \boldsymbol{\gamma}, \tilde{\mathbf{h}}(\mathbf{x}) - \boldsymbol{\xi})$. It is evident that the mapping's Jacobian is the diagonal sign matrix (± 1 on the diagonal). Thus, the map is full-rank. Finally, it is known that LICQ implies *Mangasarian-Fromovitz constraint qualification (MFCQ)*, which is equivalent to Slater's condition for convex problems [43, pp. 45, 160]. This result ensures strong duality and hence completes the proof.

C. Proof of Proposition 3

We consider the simplified version of C-OPF:

$$\mathcal{V}(\boldsymbol{\gamma}) \triangleq \min_{\mathbf{x} \in \mathbb{R}^n} f(\mathbf{x}), \quad \text{s.t.} \quad \tilde{\mathbf{g}}(\mathbf{x}) \preceq \boldsymbol{\gamma}.$$

The proof presented here generalizes to (1). Prop. 1 asserts $\nabla \mathcal{V}(\boldsymbol{\gamma}) = -\tilde{\boldsymbol{\lambda}}^* \preceq \mathbf{0}$ is unique. Let $\mathcal{F} \subseteq [\tilde{L}]$ collect the indices of false negative constraints remaining after the first *do-while* iteration in Algorithm 2. Due to the strict complementarity assumption, we have $[\tilde{\boldsymbol{\lambda}}^*]_{\mathcal{F}} \succ \mathbf{0}$. Define vector $\Delta \boldsymbol{\gamma}$, where the i -th element is given by $\Delta \boldsymbol{\gamma}_i = \mathbb{1}_{\{i \in \mathcal{F}\}}$. This vector indicates all strictly descending directions of \mathcal{V} . Thus, $\mathcal{V}(\boldsymbol{\gamma} + \epsilon \Delta \boldsymbol{\gamma}) < \mathcal{V}(\boldsymbol{\gamma})$ for all $\epsilon > 0$, and it can be shown that all constraints in \mathcal{F} are violated with respect to the original parameter $\boldsymbol{\gamma}$. Now, consider the C-OPF defined by $\lim_{\epsilon \rightarrow +\infty} \mathcal{V}(\boldsymbol{\gamma} + \epsilon \Delta \boldsymbol{\gamma})$, it violates the constraints in \mathcal{F} while its optimal objective value is strictly smaller than $\mathcal{V}(\boldsymbol{\gamma})$. We conclude the proof by observing that $\lim_{\epsilon \rightarrow +\infty} \mathcal{V}(\boldsymbol{\gamma} + \epsilon \Delta \boldsymbol{\gamma})$ is equivalent to removing all binding constraints in \mathcal{F} from $\mathcal{V}(\boldsymbol{\gamma})$.

²Henceforth, we omit the argument (\mathbf{x}) for these sets to simplify notation.